https://doi.org/10.5194/egusphere-2022-1055
Preprint. Discussion started: 14 October 2022

Quantifying vegetation indices using TLS: methodological complexities and ecological insights from a Mediterranean forest

William Rupert Moore Flynn[1], Harry Jon Foord Owen[2], Stuart William David Grieve[1,3] and Emily Rebecca Lines[2]

[1]School of Geography, Queen Mary University of London, Mile End Rd, Bethnal Green, London E1 4NS

[2]Department of Geography, University of Cambridge, Downing Place, Cambridge, CB2 3EN

[3]Digital Environment Research Institute, Queen Mary University of London, New Road, London, E1 1HH

Correspondence to: W. R. M. Flynn (w.r.m.flynn@qmul.ac.uk)

Abstract. Accurate measurement of vegetation density metrics including plant, wood and leaf area indices (PAI, WAI and LAI) is key to monitoring and modelling carbon storage and uptake in forests. Traditional passive sensor approaches, such as Digital Hemispherical Photography (DHP), cannot separate leaf and wood material, nor individual trees, and require many assumptions in processing. Terrestrial Laser Scanning (TLS) data offer new opportunities to improve understanding of tree and canopy structure. Multiple methods have been developed to derive PAI and LAI from TLS data, but there is little consensus on the best approach, nor are methods benchmarked as standard.

Using TLS data collected in 33 plots containing 2472 trees of five species in Mediterranean forests, we compare three TLS methods (*LiDAR Pulse*, *2D Intensity Image* and *Voxel-Based*) to derive PAI and compare with co-located DHP. We then separate leaf and wood in individual tree point clouds to calculate wood to total plant area (α), a metric to correct for non-photosynthetic material in LAI estimates. We use individual tree TLS point clouds to estimate how α varies with species, tree height and stand density.

We find the *LiDAR Pulse* method agrees most closely with DHP, but is limited to single scan data so cannot determine individual tree α. The *Voxel-Based* method shows promise for ecological studies as it can be applied to individual tree point clouds. Using the *Voxel-Based* method, we show that species explain some variation in α, however, height and density were stronger predictors.

Our findings highlight the value of TLS data to improve fundamental understanding of tree form and function, but also the importance of rigorous testing of TLS data processing methods at a time when new approaches are being rapidly developed. New algorithms need to be compared against traditional methods, and existing algorithms, using common reference data. Whilst promising, our results show that metrics derived from TLS data are not yet reliably calibrated and validated to the extent they are ready to replace traditional approaches for large scale monitoring of PAI and LAI.

https://doi.org/10.5194/egusphere-2022-1055
Preprint. Discussion started: 14 October 2022

1 Introduction

Terrestrial Laser Scanning (TLS) generates high-resolution 3D measurements of whole forests and individual trees (Burt et al., 2018; Disney, 2018), leading to the development of completely new monitoring approaches to understand the structure and function of ecosystems (Lines et al., 2022). Unlike traditional passive sensors, TLS can estimate plant, wood and leaf area indices (PAI; WAI; LAI) for both whole plots and individual tree point clouds (Calders et al., 2018), and is unaffected by illumination conditions. This has led to the development of several methods for processing TLS data to extract the key metrics PAI, WAI and LAI (e.g. Hosoi and Omasa, 2006; Jupp et al., 2008; Zheng et al., 2013). However, intercomparison of algorithms and processing approaches to derive the same metrics from different TLS methods are lacking.

Leaf Area Index (LAI), defined as half the amount of green leaf area per unit ground area (Chen and Black, 1992), determines global evapotranspiration, phenological patterns and canopy photosynthesis, and is therefore an essential climate variable (ECV), as well as a key input in dynamic global vegetation models (Sea et al., 2011; Weiss et al., 2004). Accurate measurements of LAI, WAI and PAI have historically been derived from labour intensive destructive sampling (Baret et al., 2013; Jonckheere et al., 2004), so over large spatial or temporal scales these can only be measured indirectly, typically with remote sensing. Large-scale remote sensing, using spaceborne and airborne instruments, has been widely used to estimate LAI over large areas (Pfeifer et al., 2012), but requires calibration and validation using in situ measurements to constrain information retrieval (Calders et al., 2018). Non-destructive in situ vegetation index estimates have historically been made by measuring light transmission below the canopy and using simplifying assumptions about canopy structure to estimate the amount of intercepting material (e.g. Beer-Lambert law; Monsi and Saeki, 1953). The most common method, Digital Hemispherical hotography (DHP; Figure 1a), requires both model assumptions and subjective user choices during data acquisition and processing in order to estimate both PAI and LAI (Breda, 2003). DHP images are processed by separating sky from canopy, but not photosynthetic from non-photosynthetic vegetative material, so additional assumptions are needed to calculate either LAI or WAI (Jonckheere et al., 2004; Pfeifer et al., 2012). Separation of LAI from PAI can be achieved by removing or masking branches and stems from hemispherical images (e.g. Sea et al., 2011; Woodgate et al., 2016), but is not reliable when leaves are occluded by woody components (Hardwick et al., 2015). An alternative approach is to take separate DHP measurements in both leaf on and leaf off conditions, and derive empirical wood to plant ratios (WAI/PAI, α) (Leblanc and Chen, 2001), but this is not always practical, for example in evergreen forests. The difficulty of separation means that studies often omit correcting for the effect of WAI on optical PAI measurements altogether (Woodgate et al., 2016), but since woody components in the forest canopy can account for more than 30% of PAI (Ma et al., 2016) this can introduce overestimation. Further, although DHP estimates of LAI or PAI are valuable both for ecosystem monitoring and developing satellite LAI products (Hardwick et al., 2015; Pfeifer et al., 2012), they are limited to sampling only at a neighbourhood or plot level (Hardwick et al., 2015; Pfeifer et al., 2012, Weiss et al., 2004), and cannot be used to measure individual tree LAI except for open grown trees (Béland et al., 2014).

The ratio of wood to total plant area, α, is known to be dynamic, changing in response to abiotic and biotic conditions. For example, the Huber value (sapwood to leaf area ratio, a related measure to α) may vary according to water availability (Carter and White 2009). Leaf area may therefore be indicative of the drought tolerance level of a tree, with more drought tolerant species displaying a lower leaf area, reducing the hydraulic conductance of

https://doi.org/10.5194/egusphere-2022-1055
Preprint. Discussion started: 14 October 2022

the whole tree and therefore increasing its drought tolerance (Niinemets and Valladares, 2006). α has been hypothesised to increase with the size of a tree in response to the increased hydraulic demand associated with greater hydraulic resistance of tall trees (Magnani et al., 2000) and higher transpiration rates of larger LAI (Battaglia et al., 1998; Phillips et al., 2003). Stand density may also impact α (Long and Smith, 1988; Whitehead, 1978), as increased stand level water use scales linearly with LAI (Battaglia et al., 1998; Specht and Specht, 1989), reducing water availability to individual trees competing for the same resources (Jump et al., 2017). Large scale quantification of α or Huber value, however, is difficult as studies usually rely on a small number of destructively sampled trees (e.g. Carter and White, 2009; Magnani et al., 2000), litterfall traps (e.g. Phillips et al., 2003) or masking hemispherical images (e.g. Sea et al., 2011; Woodgate et al., 2016). These approaches are only applicable on a small to medium scale, and in the case of image masking, cannot differentiate between individuals. Variation in α, for example by species and or stand structure, is therefore largely unknown.

1.2 TLS methods for calculating PAI, LAI and WAI

TLS methods for extracting PAI, LAI and WAI can be broadly categorised into two types: (1) LiDAR return counting, using single scan data (e.g., the *LiDAR Pulse* method; Jupp et al., 2008, and *2D Intensity Image* method; Zheng et al., 2013) and (2) point cloud voxelisation, usually using co-registered scans (e.g., the *Voxel-Based* method; Hosoi and Omasa, 2006).

The *LiDAR Pulse* method (Jupp et al., 2008; Figure 1b) estimates gap fraction (*Pgap*) using single scan data, as a function of the total number of outgoing LiDAR pulses from the sensor and the number of pulses that are intercepted by the canopy. This method, which eliminates illumination impacts associated with the use of DHP (Calders et al., 2014), has been implemented in the python module, *PyLidar* (www.pylidar.org) and the R package, *rTLS* (Guzman, et al. 2021). Using the *LiDAR Pulse* method, Calders et al. (2018) compared TLS PAI estimates from two ground-based passive sensors (LiCOR LAI-2000 and DHP) with TLS data collected with a RIEGL VZ-400 TLS in a deciduous woodland, and found the two passive sensors underestimated PAI values compared to TLS, with differences dependent on DHP processing and leaf on/off conditions.

The *2D Intensity Image* method (Zheng et al., 2013; Figure 1c), also uses raw single scan TLS point clouds, but unlike the *LiDAR Pulse* method, this approach converts LiDAR returns into 2D panoramas where pixel values represent intensity. PAI is estimated by classifying pixels as sky or vegetation, based on their intensity value, to estimate *Pgap*, and then applying Beer-Lambert's law. As for the *LiDAR Pulse* method, this approach has been shown to generate higher PAI estimates than DHP (Calders et al., 2018; Woodgate et al., 2015; Grotti et al., 2020), with differences attributed to the greater pixel resolution and viewing distance of TLS resolving more small canopy details (Grotti et al., 2020).

The *Voxel-Based* method (Figure 1d) estimates PAI by segmenting a point cloud into voxels and either simulating radiative transfer within each cube (Béland et al., 2014; Kamoske et al., 2019), or classifying voxels as either containing vegetation or not, and dividing vegetation voxels by the total number of voxels (Hosoi and Omasa, 2006; Itakura and Hosoi, 2019; Li et al., 2017). Crucially, this method may be applied to multiple co-registered scan point clouds and so can be used to calculate PAI for both whole plots and individual, segmented TLS trees.

https://doi.org/10.5194/egusphere-2022-1055
Preprint. Discussion started: 14 October 2022

The *LiDAR Pulse* method and *2D Intensity Image* method both use single scan data. However, to generate robust estimates of canopy properties that avoid errors from occlusion effects, multiple co-registered scans taken from different locations are likely needed (Wilkes et al., 2017). Further, both these methods require raw unfiltered data to accurately measure the ratio of pulses emitted from the scanner and number of pulses that are intercepted by vegetation. This means "noisy" points caused by backscattered pulses (Wilkes et al., 2017) are included in analyses, potentially leading to higher PAI estimates. However, the *LiDAR Pulse* and *2D Intensity Image* methods may introduce fewer estimation errors compared DHP, which is influenced by differences in sky illumination conditions and camera exposure (Weiss et al., 2004).

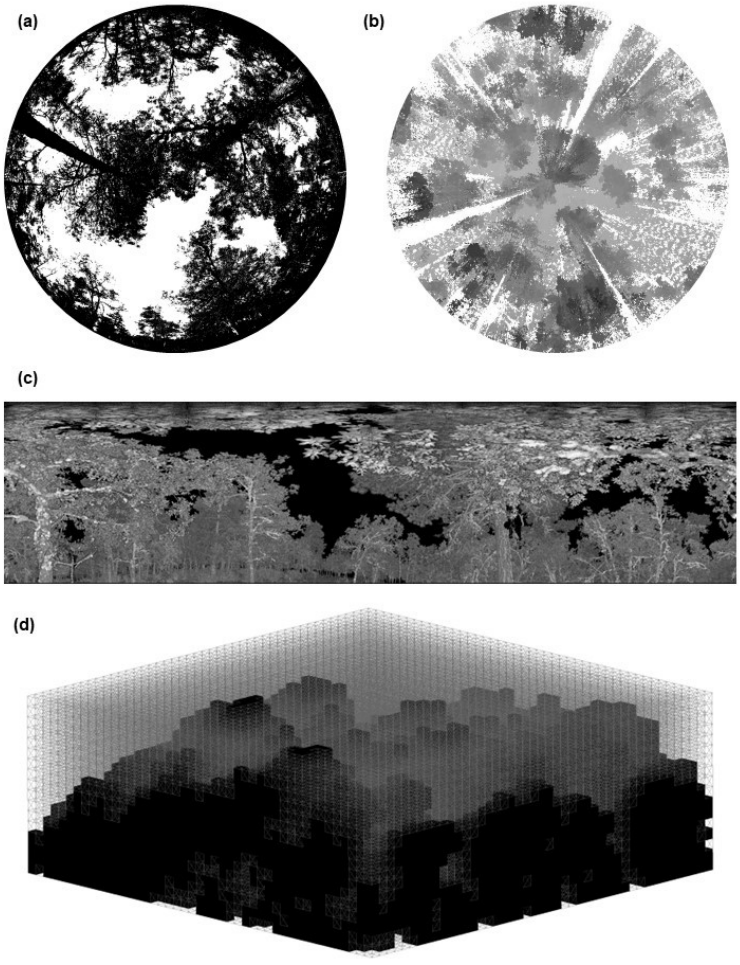

Figure 1: Methods for PAI estimation applied in this study: (a) a binarised digital hemispherical photograph (DHP), (b) TLS raw single scan point cloud, used within the LiDAR Pulse method (Jupp et al., 2008)**. Image shows a top-down view of raw point cloud and greyscale represents low (grey) and high (black) Z values, (c) TLS 2D intensity image for the 2D Intensity Image method** (Zheng et al., 2013)**, (d) Voxelised co-registered whole plot point cloud for the Voxel-Based method** (Hosoi and Omasa, 2006)**, showing a representative schematic of cube voxels with edge length of 1m,**

https://doi.org/10.5194/egusphere-2022-1055
Preprint. Discussion started: 14 October 2022

voxelised using the *R* package *VoxR* (Lecigne et al., 2018)**. Solid black voxels are classified as containing vegetation (filled) and voxels outlined with grey lines are voxels classified as empty.**

1.3 Scope and aims

In this study we use a dataset of 528 co-located DHP and high-resolution TLS scans from 33 forest plots to compare DHP derived PAI with estimates from three methods to estimate PAI from TLS data: the *LiDAR Pulse* method; the *2D Intensity Image* method and the *Voxel-Based* method (Figure 1). We use a dataset collected from a network of pine/oak forest plots in Spain (Owen et al., 2021) and ask **(1)** are the three TLS methods able to reproduce DHP PAI estimates at single scan and whole plot level? **(2)** does α, calculated from the *Voxel-Based* method on individual tree point clouds, vary with species and tolerance to drought; and **(3)** does α scale with height and stand density?

2. Methods

2.1 Study site

We collected TLS and DHP data from 29 plots in Alto Tajo Natural Park (40°41′N 02°03′W; FunDIV plots; Baeten et al., 2013) and four plots in Cuellar (41°23′N 4°21′W) in June - July 2018 (see Owen et al., 2021 for full details). Plots contained two oak species: semi-deciduous *Q. faginea* and evergreen *Q. ilex,* and three pine species: *P. nigra, P. pinaster* and *P. sylvestris*. *P. sylvestris* is the least drought tolerant species, followed by *P. nigra, Q. faginea*, *Q. ilex*; shade tolerance follows the same ranking (Niinemets and Valladares, 2006; Owen et al., 2021). Although not quantitatively ranked, *P. pinaster* has been shown to be very drought tolerant, appearing in drier areas than the other species (Madrigal-González et al., 2017). The area is characterised by a Mediterranean climate (altitudinal gradient 840 – 1400 m.a.s.l.) (Jucker et al., 2014; Madrigal-González et al., 2017). In addition to the five main canopy tree species, plots contained an understory of *Juniperus thurifera* and *Buxus sempervirens* (Kuusk et al., 2018).

2.2 Field protocol

In each of the 33 30 x 30 m plots we collected TLS scans on a 10 m grid, making 16 scan locations following Wilkes et al., (2017) to minimise occlusion effects associated with insufficient scans. We used a Leica HDS6200 TLS set to super high resolution (3.1 x 3.1mm resolution at 10 m with a beam divergence of ≤ 5 mm at 50 m; scan time 6m 44 s; see Owen et al., 2021). At each of the 528 scan locations and following the protocol in Pfeifer et al., (2012), we captured co-located DHP images with three exposure settings (automatic and ± one stop exposure compensation), levelling a Canon EOS 6D full frame DSLR sensor with a Sigma EX DG F3.5 fisheye lens, mounted on a Vanguard Alta Pro 263AT tripod.

2.3 Calculation of single scan and whole plot PAI using DHP data

For each of the red-green-blue (RGB) DHP images we extracted the blue band for image thresholding, as this best represents sky/vegetation contrast (Pfeifer et al., 2012). For each plot, we picked the exposure setting that best represented sky/ vegetation difference based on pixel brightness histograms of four sample locations indicative of the plot. We carried out automatic image thresholding using the Ridler and Calvard method (1978), to create a binary image of sky and vegetation, avoiding subjective user pixel classification (Jonckheere et al., 2005). We calculated PAI from the binary image, limiting the field of view to a 5° band centred on the hinge angle of 57.5°

https://doi.org/10.5194/egusphere-2022-1055
Preprint. Discussion started: 14 October 2022

(55° – 60°). The hinge angle has a path length through the canopy twice the canopy height, so the band around it is an area of significant spatial averaging taken as representative of canopy structure of the area (Calders et al., 2018; Jupp et al., 2008). From the binarised hinge angle band we calculated gap fraction as the number of sky pixels divided by the total number of pixels and PAI using an inverse Beer-Lambert law equation (Monsi and Saeki, 1953). We calculated whole plot PAI as the arithmetic mean within plot scan location PAI. As this value does not correct for canopy clumping, it is better described as effective PAI, rather than true PAI (Woodgate et al., 2015). However, as the TLS and DHP methods we apply here account for canopy clumping differently, we compare effective values and here-on refer to effective PAI as PAI (Calders et al., 2018).

2.4 Calculation of single scan and whole plot PAI from TLS data

To calculate PAI using the *LiDAR Pulse* method (Jupp et al., 2008), we calculated the gap fraction (*Pgap*) for a single scan (Figure 1b) by summing all returned laser pulses and dividing by the number of total outgoing pulses, following Lovell et al. (2011; see Eq. 7 in that study), and then estimated PAI following Jupp et al. (2008; see Eq. 18 in that study), setting the sensor range to 5° around the hinge angle as before (55° – 60°). Single scan PAI was taken as the cumulative sum of PAI values estimated by vertically dividing the hinge region into 25 cm intervals (Calders et al., 2014). We implemented the *LiDAR Pulse* method using the open-source *R* (R Core Team, 2020) package, *rTLS* (Guzmán and Hernandez, 2021).

To calculate PAI using the *2D Intensity Image* method (Zheng et al., 2013) we converted 3D TLS point cloud data from all 528 scan locations into polar coordinates and scaled intensity values to cover the full 0-255 range (Figure 1c) and rasterised into a 2D intensity image using the open-source *R* package, *raster* (Hijmans, 2022). We cut the 2D intensity image to a 5° band around the hinge angle (55° – 60°) and classified sky and vegetation pixels in each image using the Ridler and Calvard method (1978). We calculated *Pgap* as the number of pixels classified as sky divided by the total number of pixels and derived PAI with an inverse Beer-Lambert law equation (Monsi and Saeki, 1953).

Following the same approach as applied to our DHP data, we calculated whole plot PAI for the *LiDAR Pulse* and *2D Intensity Image* methods as the arithmetic mean of within plot single scan PAI estimates.

To calculate PAI using the *Voxel-Based* method, we followed a voxel classification approach (Hosoi and Omasa, 2006), matching the voxel size to the resolution of the point cloud (0.05 m), following Li et al., (2017), who showed that matching the voxel size to the point cloud point to point minimum distance (resolution) increases accuracy as small canopy gaps are not included in voxels classified as vegetation. We combined individually segmented trees (see Owen et al., 2021) into whole plot point clouds and voxelised them using the open source *R* package, *VoxR* (Lecigne et al., 2018), with a full grid covering the minimum to maximum XYZ ranges of the plot. We classified any voxel containing > 0 points as vegetation ("filled"), and empty voxels as gaps. We then split the voxelised point cloud into slices one voxel high. Within each slice, the contact frequency is calculated as the fraction of filled to total number of voxels. We then multiplied the contact frequency by a correction factor for leaf inclination, set at 1.1 (Li et al., 2017), and whole plot PAI was calculated as the sum of all slices' contact frequencies.

https://doi.org/10.5194/egusphere-2022-1055
Preprint. Discussion started: 14 October 2022

2.5 Calculation of individual tree PAI, WAI and α using the voxel-based method

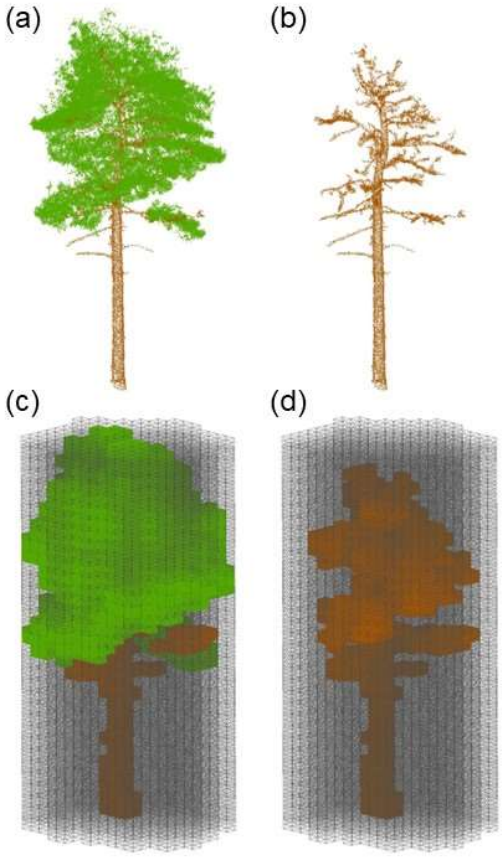

Figure 2: Visualisation of the workflow for applying the Voxel-Based method to estimate individual-tree PAI, WAI and *α*. (a) Individual tree point cloud; (b) separated leaf off (wood) individual tree point cloud; (c) voxelised individual tree point cloud; (d) voxelised wood cloud. Solid black voxels are filled voxels and grey lines are empty voxels. Empty voxels occupy the space within the projected crown area of the tree. Image shows schematic of point cloud voxelised with cube voxels with edge length of 0.5 m. Wood and leaf separation was carried out using *TLSeparation* (Vicari et al., 2019). Point cloud voxelisation was carried out using modified functions from *R* package *VoxR* (Lecigne et al., 2018).

As the only method using multiple co-registered scans, the *Voxel-Based* method is only method we found capable of estimating individual tree leaf and wood properties. We estimated PAI and WAI for 2472 individual trees segmented from co-registered point clouds following a similar method to the whole plot point cloud. We extracted individual trees using the automated tree segmentation program *treeseg* (Burt et al., 2019), implemented in C++, see Owen et al., (2021) for full details, and Owen et al., (2022) for individual segmented tree data.

To estimate PAI, WAI and α for each tree, we first separated leaf from wood points in individual tree point clouds using the open source Python library *TLSeparation* (Vicari et al., 2019), and then used the wood only point clouds to calculate WAI. *TLSeparation* classifies points as leaf or wood, iteratively looking at a predetermined number of nearest neighbours (*knn*). The *knn* of each iteration is directly dependent on point cloud density, since high

https://doi.org/10.5194/egusphere-2022-1055
Preprint. Discussion started: 14 October 2022

density point clouds will require higher a *knn* (Vicari et al., 2019). We used the utility package in *TLSeparation* to automatically detect the optimum *knn* for each tree point cloud.

To voxelise individual tree complete (Figure 2a) and wood only (Figure 2b) point clouds, we used a modified approach based on Lecigne et al., (2018), voxelising within the projected crown area of the whole tree point cloud (Figure 2c) to calculate PAI. We calculated WAI within the projected crown area of the whole tree (Figure 2d; using the whole crown and not just the wood point cloud), and derived α for each tree as $^{WAI}/_{PAI}$.

2.6 Statistical Analyses

We tested the relationships between TLS PAI and DHP PAI estimates using Standardised Major Axis (SMA) using the open source *R* (R Core Team, 2020) package, *smatr* (Warton et al., 2012). SMA is an approach to estimating a line of best fit where we are not able to predict one variable from another (Warton et al., 2006); we chose SMA because we do not have a 'true' validation dataset, so avoid assuming either DHP or any of the TLS methods produces the most accurate results. For each TLS method, we assessed the relationship with DHP using the coefficient of determination and RMSE. To further understand observed drivers of variance in PAI, we tested the relationship between PAI and TLS estimated whole plot crown area index, CAI, calculated as the sum of projected crown area, divided by the plot area (Owen et al., 2021), and indicative measure of stand density, using SMA.

To test if α differs by species, we used linear mixed models (LMMs) in the *R* package, *lme4* (Bates et al., 2015). We included an intercept only random plot effect to account for local effects on α:

$$\alpha_{i,sj} = a_s + Plot_j \quad (1)$$

here, α_i is α of an individual of species *s,* in plot *j*, and a_s is the parameter to be fit. To test the effect of stand structure and tree height on α we fit relationships separately for each species, again including a random plot effect:

$$\alpha_{i,sj} = a_s + b_s H_i + c_s CAI_j + Plot_{sj} \quad (2)$$

here H_i is the height of the tree, CAI_j is the crown area index for the plot, with other parameters as before.

For each species' model (equation 2), we calculated the intra-class correlation coefficient (ICC). The ICC, similar to coefficient of determination, quantifies the amount of variance explained by the random effect in a linear mixed model (Nakagawa et al., 2017).

https://doi.org/10.5194/egusphere-2022-1055
Preprint. Discussion started: 14 October 2022

3. Results

3.1 Comparison of plant area index estimated by DHP and single scan TLS

Of the two single scan TLS methods tested (*LiDAR Pulse* method and *2D Intensity Image* method), we found that PAI estimated using the *LiDAR Pulse* method more strongly agreed with DHP PAI, but there was also significant correlation for the *2D Intensity Image* method (SMA; *LiDAR Pulse* method $R^2 = 0.50$, slope = 0.73, $p<0.001$, RMSE = 0.14, and *2D Intensity Image* method $R^2 = 0.22$, slope = 0.38, $p<0.001$, RMSE = 0.39, respectively, Figure 3a). At larger PAI values, both TLS methods underestimated PAI compared with DHP (Figure 3b). We found statistically significant negative correlations between residuals and DHP for both methods (SMA; *2D Intensity Image* method residuals $R^2 = 0.85$, slope = -0.88, $p<0.01$; *LiDAR Pulse* method residuals $R^2 = 0.47$, slope = -0.70, $p<0.01$; Figure 3b). The *2D Intensity Image* method showed larger underestimation at higher DHP PAI values, suggesting this method may saturate sooner than both DHP and the *LiDAR Pulse* method at higher PAI values (Figure 3b).

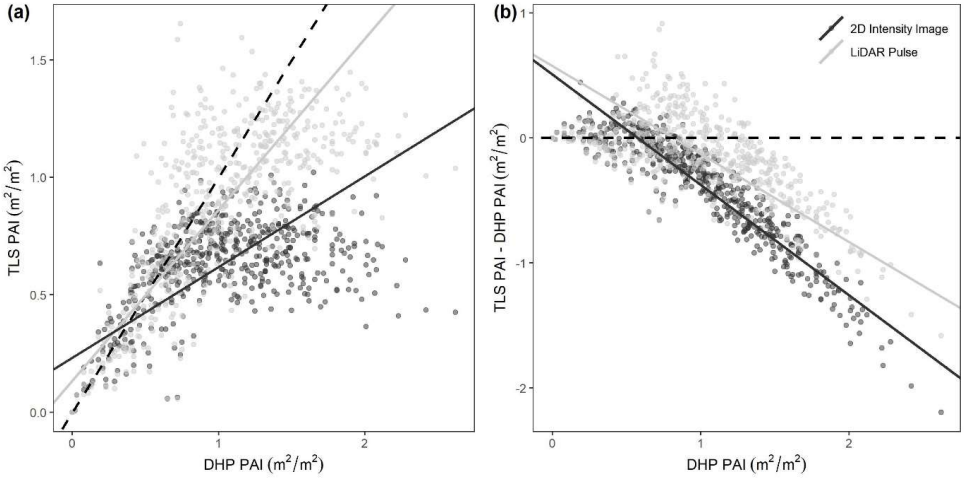

Figure 3: Comparison of single scan TLS PAI and DHP PAI estimates, for all 528 scan locations (16 per plot). (a) The correlation between DHP derived PAI with PAI derived using the 2D Intensity Image method, and LiDAR Pulse method. Dashed line represents 1:1 relationship. (b) The difference between TLS and DHP PAI estimates for the 2D Intensity Image method, and LiDAR Pulse method (dashed line at 0). Lines show statistically significant relationships fitted using SMA ($p<0.01$).

3.2 Comparison of whole plot plant area index estimated using TLS and DHP and the effect of plot structure on PAI

We found statistically significant correlations between TLS whole plot PAI values and DHP PAI for all three TLS methods. As for single scans (Figure 3), the *LiDAR Pulse* method showed the closest agreement to DHP PAI, here compared to both the *Voxel-Based* and *2D Intensity Image* methods (SMA; *LiDAR Pulse* method $R^2 = 0.66$, slope = 0.82, $p<0.01$, RMSE = 0.14; *Voxel-Based* method $R^2 = 0.39$, slope = 2.76, $p<0.01$, RMSE = 0.88; *2D Intensity Image* method $R^2 = 0.35$, slope = 0.36, $p<0.01$, RMSE = 0.39, respectively; Figure 4a). The *2D Intensity Image* method and *LiDAR Pulse* method consistently underestimated PAI compared to DHP, whilst the *Voxel-Based* method underestimated in plots with lower DHP PAI and overestimated in plots with higher DHP PAI. The *Voxel-*

https://doi.org/10.5194/egusphere-2022-1055
Preprint. Discussion started: 14 October 2022

Based method's high PAI values compared to other methods is likely due to its use of multiple co-registered scans reducing occlusion effects prevalent in single scan data.

To assess the effect of plot structure on variation in TLS derived PAI, we compared TLS PAI estimates to TLS estimated crown area index (CAI, m^2 projected crown area per m^2 ground area, Figure 4b). We found a significant positive relationship between CAI and PAI estimated using each of the *LiDAR Pulse* method, the *Voxel-Based* method, and DHP (SMA*; LiDAR Pulse* method $R^2 = 0.79$, slope = 1.69, $p<0.01$; *Voxel-Based* method $R^2 = 0.76$, slope = 5.72, $p<0.01$; *2D Intensity Image* method R2 = 0.15, slope = 0.76; DHP $R^2 = 0.46$, slope = 2.07, $p<0.01$, respectively; Figure 4b), where the *2D Intensity Image* method appears to saturate at medium CAI values (Figure 4b).

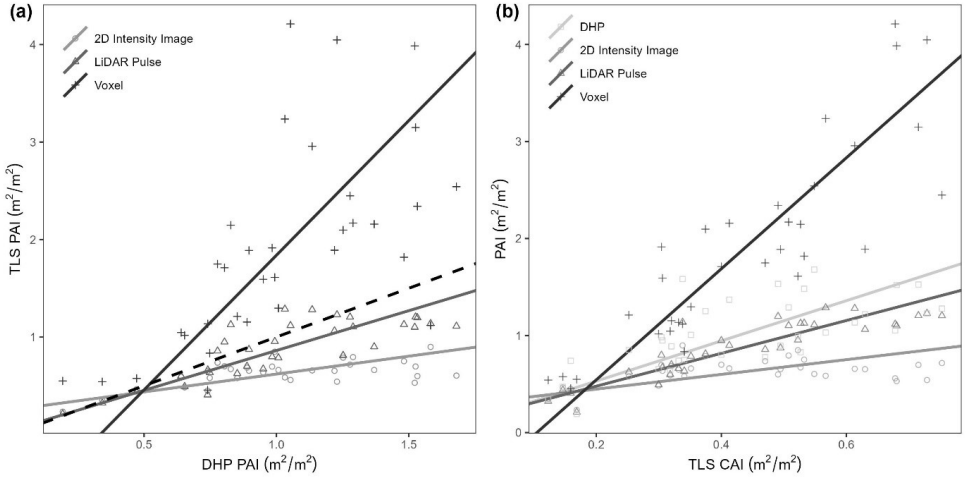

Figure 4: Comparison of plot level TLS PAI and DHP PAI, and CAI vs PAI estimates for all 33 plots. (a) The correlation between DHP derived PAI and PAI derived using 2D Intensity Image (circle), LiDAR Pulse (triangle) and Voxel-Based (cross) methods (b) The correlation between TLS derived CAI and PAI derived using DHP (square), LiDAR Pulse (triangle) and Voxel-Based (cross) methods. Lines show statistically significant relationships fitted using SMA (p<0.01). Dashed line represents 1:1 relationship.

3.4 Influence of species, tree height and CAI on α

To understand drivers of variance in α, we used individual tree PAI and WAI, calculated using the *Voxel-Based* method to test the relationship between species and α, and height/ CAI and α. We found that more drought tolerant species generally had higher α values than less drought tolerant species (Table A1; Figure 5), however, confidence intervals were wide and overlapping, suggesting that species is not a strong predictor of variation in α. We found a statistically significant negative effect of height ($p<0.001$; Table A2; Figure 6a) and positive effect of CAI ($p<0.01 – 0.05$; Table A2; Figure 6b) on α for all species apart from *P. sylvestris*. α decreased more rapidly with height and increased less rapidly with CAI for oaks than pines. Statistically significant ICC values were higher for *P. nigra* (ICC = 0.211; Table A2) than *P. pinaster, Q. faginea* and *Q. ilex* (ICC = 0.036; 0.060; 0.070,

https://doi.org/10.5194/egusphere-2022-1055
Preprint. Discussion started: 14 October 2022

292 respectively), showing that more α variation is explained by the random plot effect in *P. nigra* than the other
293 species. *P. pinaster* has a wider confidence interval (Figure 5), possibly explained by its lower sample size.

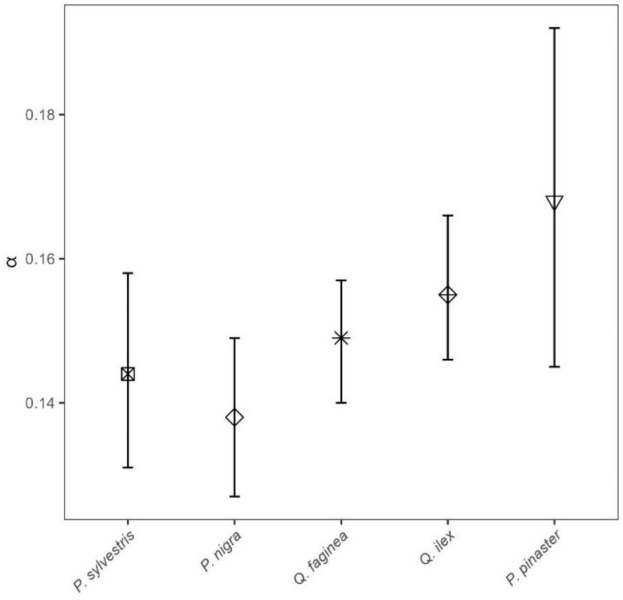

294 **Figure 5: Linear mixed model derived α values (a, equation 1) for all 2472 individual trees of species *P. sylvestris, P.***
295 ***nigra, Q. faginea, Q. ilex* and *P. pinaster*. Error bars represent 95% confidence intervals. Species are listed from low –**
296 **high drought tolerance, with the exception of *P. pinaster*, for which drought tolerance index has not been calculated in**
297 **the literature.**

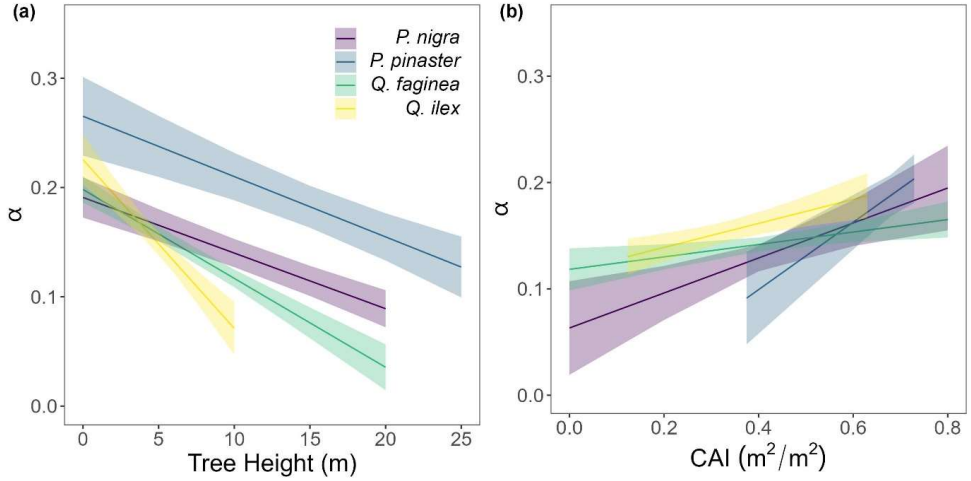

298 **Figure 6: Variation in α for each species: *Pinus nigra, P. pinaster, Q. faginea* and *Q. ilex* with (a) height and (b) plot**
299 **CAI. Lines represent statistically significant linear mixed models (equation 2; $p < 0.001$). Ribbons represent 95%**
300 **confidence intervals. The model for *P. sylvestris* was not statistically significant.**

301

302

303

https://doi.org/10.5194/egusphere-2022-1055
Preprint. Discussion started: 14 October 2022

4. Discussion

4.1 Comparison of approaches to deriving PAI from remote sensed data

We found substantial differences in PAI values estimated from TLS and DHP and from different TLS processing methods (Figures 3 and 4). Further, differences between TLS methods varied across plot structure (CAI), with the greatest differences between methods in plots with high CAI, and therefore high canopy density. Although previous studies have presented TLS as an improvement over DHP due to its independence of illumination and sky conditions during the data acquisition phase, and ability to resolve fine-scale canopy elements and gaps (Calders et al., 2018; Grotti et al., 2020; Zhu et al., 2018), we have shown that there is large variability between TLS processing methods in Mediterranean forests. Rigorous intercomparison of approaches, ideally using standard benchmarking TLS datasets, and destructive sampling, would improve trust and reliability of TLS algorithms.

4.2 The *LiDAR Pulse* and *2D Intensity Image* method derived PAI estimates were lower than those derived from DHP and the *Voxel-Based* method

We found the *LiDAR Pulse* method (Jupp et al., 2008) to have the best agreement with DHP for both whole plot and single scan PAI estimates. In contrast to previous TLS – DHP comparisons (Calders et al., 2018; Grotti et al., 2020; Woodgate et al., 2015), we found that the *LiDAR Pulse* and *2D Intensity Image* methods underestimated PAI compared to DHP, except at very low PAI values. Quantification of PAI from DHP may introduce additional sources of error, for example, its relatively lower resolution compared to TLS could lead to mixed pixels that have a greater chance of misclassification of sky as vegetation (Jonckheere et al., 2004). This effect could be enhanced in a Mediterranean forest as trees in drier climates tend to have smaller leaves (Peppe et al., 2011), leading to more small canopy gaps that TLS may resolve where DHP cannot. Further, although we took steps to reduce the error introduced at DHP data acquisition and processing steps, including using automatic thresholding and collecting images with multiple exposures, DHP processing requires both model and user assumptions that can impact results. For example, DHP PAI estimates are highly sensitive to camera exposure; increasing one stop of exposure can result in 3 – 28% difference in PAI and use of automatic exposure can result in up to 70% error (Zhang et al., 2005).

We found the *Voxel-Based* method overestimated PAI values compared to the other methods at the whole plot level. This is likely due to the method's use of co-registered scans, rather than averaged single scan PAI values, since co-registered scans will reduce occlusion effects prevalent in single scan data that could to lead to an underestimation of PAI (Wilkes et al., 2017). The *Voxel-Based* method is, however, sensitive to voxel size (Li et al., 2016), and larger voxels lead to larger PAI estimates as they fill small canopy gaps; we chose a voxel size of 0.05 m to match the minimum distance between points in our downsampled dataset. However, the *Voxel-Based* method is a memory intensive approach to calculating PAI, and smaller voxels have higher memory requirements. We picked this data resolution, and therefore voxel size, to balance the need to capture fine-scale canopy details against memory requirements for running many large plots. Voxel size could have been chosen based on estimates' match to DHP, but this would assume (1) that DHP estimates are most accurate, and (2) that DHP data are always available, limiting the wider applicability of our findings. Understanding which method is over or underestimating would require a destructively sampled dataset for validation, which was not possible for this study (or most ecosystems). However, other studies using voxel approaches have found that although these

https://doi.org/10.5194/egusphere-2022-1055
Preprint. Discussion started: 14 October 2022

produce high LAI values for individual trees, these are underestimates compared with destructive samples (Li et al., 2016). Regardless, PAI and LAI estimates using a *Voxel-Based* approach are highly dependent on voxel size (Béland et al., 2014), and future work should test the influence of voxel size on PAI estimates, using destructive samples in a range of environments.

4.3 Relationship between PAI and CAI varied according to method and sensor

The *LiDAR Pulse* method had the strongest relationship (defined as highest R^2) with TLS derived CAI, demonstrating that the method is well suited to measuring PAI across the range of plot CAI values used in this study. Although the *2D Intensity Image* method can tackle the significant challenges presented by edge effects and partial beam interceptions, particularly present in phase-shift systems (Grotti et al., 2020), our results suggest this method has a lower performance ability, with saturation occurring sooner than all other methods in dense forests (Figures 3 and 4). The *2D Intensity Image* method uses the same raw single scan data as the *LiDAR Pulse* method, so the better performance from the latter is likely due to the method's use of vertically resolved gap fraction; both the *LiDAR Pulse* method and *Voxel-Based* method account for the vertical structure of the canopy by summing vertical slices through the canopy.

4.4 α variation between species and plot

We used the *Voxel-Based* method to investigate individual tree α variation between species and across structure, as this was the only approach we identified that could be applied to single tree point clouds. We found α values obtained were within the range of values obtained from destructive approaches (0.1 – 0.6, Gower et al., 1997). The drought and shade intolerant *P. nigra* showed stronger variability in α across plots (higher ICC value, Table A2) than other species, suggesting its wood – leaf ratio may be more sensitive to site factors. However, as the plots measured in this study vary in both abiotic conditions (altitude, aspect, slope, wetness) as well as species composition, stem density and canopy cover, there may be other drivers of variation in α values.

We found some evidence that species with higher drought tolerance had higher α values (Figure 5; Table A1), however, confidence intervals were wide, suggesting a weak relationship. There is evidence that trees that tolerate water limited environments have a lower leaf area (Battaglia et al., 1998; Mencuccini and Grace, 1995), so higher α values may reflect maintenance of homeostasis of leaf water use through adjustment of wood to leaf area ratio (Carter and White, 2009; Gazal et al., 2006). The potential for a tree to lose water is mostly regulated through leaf traits including stomatal conductance and leaf area, and both stand (Battaglia et al., 1998; Specht and Specht, 1989) and individual tree (Mencuccini, 2003) water use have been found to scale linearly with LAI, with drought often mitigated through leaf shedding (López et al., 2021).

4.5 Tree stature and stand density drives α variation

Although species explain some variation in α, tree height and plot CAI were stronger predictors for all species, showing the importance of local stand structure on leaf and woody allocation. We found that α scaled negatively with height for all species apart from *P. sylvestris,* suggesting that in this environment, taller trees generally have a lower proportion of wood to plant area index than shorter ones. *P. sylvestris,* which is at the edge of its geographical range and physiological limits (Castro-Díez et al., 1997; Owen et al., 2021), showed no significant relationship between height and α. We found that α scaled positively with plot level CAI for all species apart from *P. sylvestris,* that is, trees growing in denser plots have a higher α. This supports theory that trees growing in dense

https://doi.org/10.5194/egusphere-2022-1055
Preprint. Discussion started: 14 October 2022

forests are competing for resources, reducing individual tree leaf area (Jump et al., 2017). The negative height – α and positive CAI – α relationships in our model suggest that trees may initially invest in vertical growth to reach the canopy level, and once there invest in lateral growth, with more leaf area, to increase light capture. This supports theory that trees grow to outcompete neighbouring individuals for light capture (Purves and Pacala, 2008) and evidence that both lateral growth and LAI are reduced beneath closed canopies (Beaudet and Messier, 1998; Canham, 1988).

Wood may be harder to accurately classify than leaves in TLS data (Vicari et al., 2019), resulting in a higher occurrence of false positives in wood clouds, potentially leading to an overestimation in WAI, and therefore underestimation of α, especially in trees with small leaves which are prevalent in dry, Mediterranean environments (Peppe et al., 2011). The problem of misclassification will increase in taller trees due to TLS beam divergence, occlusion and larger beam footprint at further distances (Vicari et al., 2019), suggesting that WAI overestimation could be more pronounced in tall trees. Although our dense scanning strategy (Owen et al., 2021) was designed to mitigate some of these effects, it is possible our findings could underestimate the slope of the negative relationship between α and tree height.

4.6 Correcting for non-photosynthetic elements in LAI estimates using TLS

The value of TLS data to estimate individual tree PAI, WAI and subsequently α, demonstrates their potential to corrective factors for non-photosynthetic components in ground based remote sensing measurements of LAI. Properly correcting for WAI in LAI estimates is of global importance as small errors in ground based measurements propagate through to large scale satellite observations generating large errors in global vegetation models (Calders et al., 2018). Our results echo others' in finding that the prevalence of woody material in the tree canopy, and therefore α, is dynamic and varies by species as well as senescence, crown health and, in the case of deciduous forests, leaf phenology (Gower et al., 1999). The use of single α value in a plot or region (Olivas et al., 2013; Woodgate et al., 2016), invariant of species, size and forest structure, to convert PAI to LAI is therefore problematic (Niu et al., 2021). Our study demonstrates the importance of taking species mix and structural variation into account when correcting for non-photosynthetic material in ground-based LAI estimates.

5. Conclusions

We tested three methods for estimating PAI using Terrestrial Laser Scanning data and compared these against traditional DHP measurements. We found large variation between PAI values estimated from each TLS method and DHP, demonstrating that care should be taken when deriving PAI from ground based remote sensing methods. Although the *LiDAR Pulse* method was found to have the best agreement with both single scan and whole plot PAI values measured by DHP, the *Voxel-Based* method allowed separate analysis of the key metric used to correct for the effect of WAI in LAI measurements, α, in individual trees. We recommend the *LiDAR Pulse* method as a fast and effective method for PAI estimation independent of illumination conditions. Whilst the *Voxel-Based* method may be used to analyse individual tree α and determine ecological drivers of variation, work remains to determine the validity of these approaches, in particular correct voxel size choice. We found that α varies by species, height and stand density, showing the importance of accurately correcting for WAI on the individual tree level and the utility of TLS to do so.

https://doi.org/10.5194/egusphere-2022-1055
Preprint. Discussion started: 14 October 2022

The variation in our results for the different methods used to derive PAI from TLS data show that there is some way to go before TLS derived vegetation indices can be interpreted as robust and reliable. Validation using destructive samples and further intercomparison studies of methods are needed to demonstrate the advantages of TLS, and use of benchmarking datasets should be standard. DHP is a faster, cheaper and more widely accessible method for PAI estimation, and while TLS promises to alleviate potential bias in DHP estimates, results are highly methods dependent. Our results demonstrate the challenges that stand in the way of large scale adoption of TLS for vegetation indices monitoring.

6. Code availability

See https://github.com/will-flynn/tls_dhp_pai.git for all processing and modelling code.

7. Data availability

See Owen et al., (2022) for individual segmented tree data.

8. Author contribution

All authors designed the study. HJFO and WRMF collected and processed TLS and DHP data; WRMF performed formal analysis with guidance from all authors. WRMF led the writing with input from all authors. All authors contributed critically to drafts and gave final approval for publication.

9. Competing interests

The authors declare that they have no conflict of interest.

7. Acknowledgements

WRMF was funded through a London NERC DTP PhD studentship. ERL, HJFO and SWDG were funded through the UKRI Future Leaders Fellowship awarded to ERL (MR/T019832/1).

References

Baeten, L., Verheyen, K., Wirth, C., Bruelheide, H., Bussotti, F., Finér, L., Jaroszewicz, B., Selvi, F., Valladares, F., Allan, E., Ampoorter, E., Auge, H., Avăcăriei, D., Barbaro, L., Bărnoaiea, I., Bastias, C. C., Bauhus, J., Beinhoff, C., Benavides, R., Benneter, A., Berger, S., Berthold, F., Boberg, J., Bonal, D., Brüggemann, W., Carnol, M., Castagneyrol, B., Charbonnier, Y., Chećko, E., Coomes, D., Coppi, A., Dalmaris, E., Dănilă, G., Dawud, S. M., de Vries, W., De Wandeler, H., Deconchat, M., Domisch, T., Duduman, G., Fischer, M., Fotelli, M., Gessler, A., Gimeno, T. E., Granier, A., Grossiord, C., Guyot, V., Hantsch, L., Hättenschwiler, S., Hector, A., Hermy, M., Holland, V., Jactel, H., Joly, F.-X., Jucker, T., Kolb, S., Koricheva, J., Lexer, M. J., Liebergesell, M., Milligan, H., Müller, S., Muys, B., Nguyen, D., Nichiforel, L., Pollastrini, M., Proulx, R., Rabasa, S., Radoglou, K., Ratcliffe, S., Raulund-Rasmussen, K., Seiferling, I., Stenlid, J., Vesterdal, L., von Wilpert, K., Zavala, M. A., Zielinski, D., and Scherer-Lorenzen, M.: A novel comparative research platform designed to determine the functional significance of tree species diversity in European forests, Persepect. Plant. Ecol., 15, 281–291, https://doi.org/10.1016/j.ppees.2013.07.002, 2013.

Baret, F., Weiss, M., Lacaze, R., Camacho, F., Makhmara, H., Pacholcyzk, P., and Smets, B.: GEOV1: LAI and FAPAR essential climate variables and FCOVER global time series capitalizing over existing products. Part1: Principles of development and production, Remote Sens. Environ., 137, 299–309, https://doi.org/10.1016/j.rse.2012.12.027, 2013.

https://doi.org/10.5194/egusphere-2022-1055
Preprint. Discussion started: 14 October 2022

455 Bates, D., Mächler, M., Bolker, B., and Walker, S.: Fitting Linear Mixed-Effects Models Using lme4, J. Sat.
456 Softw., 67, https://doi.org/10.18637/jss.v067.i01, 2015.

457 Battaglia, M., Cherry, M. L., Beadle, C. L., Sands, P. J., and Hingston, A.: Prediction of leaf area index in
458 eucalypt plantations: effects of water stress and temperature, Tree Physiol., 18, 521–528,
459 https://doi.org/10.1093/treephys/18.8-9.521, 1998.

460 Beaudet, M. and Messier, C.: Growth and morphological responses of yellow birch, sugar maple, and beech
461 seedlings growing under a natural light gradient, Can. J. Forest Res., 28, 1007–1015,
462 https://doi.org/10.1139/x98-077, 1998.

463 Béland, M., Baldocchi, D. D., Widlowski, J.-L., Fournier, R. A., and Verstraete, M. M.: On seeing the wood
464 from the leaves and the role of voxel size in determining leaf area distribution of forests with terrestrial LiDAR,
465 Agr. Forest Meterol., 184, 82–97, https://doi.org/10.1016/j.agrformet.2013.09.005, 2014.

466 Breda, N. J. J.: Ground-based measurements of leaf area index: a review of methods, instruments and current
467 controversies, J. Exp. Bot., 54, 2403–2417, https://doi.org/10.1093/jxb/erg263, 2003.

468 Burt, A., Disney, M., and Calders, K.: Extracting individual trees from lidar point clouds using treeseg, Methods
469 Ecol. Evol., 10, 438–445, https://doi.org/10.1111/2041-210X.13121, 2019.

470 Calders, K., Armston, J., Newnham, G., Herold, M., and Goodwin, N.: Implications of sensor configuration and
471 topography on vertical plant profiles derived from terrestrial LiDAR, Agr. Forest Meterol., 194, 104–117,
472 https://doi.org/10.1016/j.agrformet.2014.03.022, 2014.

473 Calders, K., Origo, N., Disney, M., Nightingale, J., Woodgate, W., Armston, J., and Lewis, P.: Variability and
474 bias in active and passive ground-based measurements of effective plant, wood and leaf area index, Agr. Forest
475 Meterol., 252, 231–240, https://doi.org/10.1016/j.agrformet.2018.01.029, 2018.

476 Canham, C. D.: Growth and Canopy Architecture of Shade-Tolerant Trees: Response to Canopy Gaps, Ecology,
477 69, 786–795, https://doi.org/10.2307/1941027, 1988.

478 Carter, J. L. and White, D. A.: Plasticity in the Huber value contributes to homeostasis in leaf water relations of
479 a mallee Eucalypt with variation to groundwater depth, Tree Physiol., 29, 1407–1418,
480 https://doi.org/10.1093/treephys/tpp076, 2009.

481 Castro-Díez, P., Villar-Salvador, P., Pérez-Rontomé, C., Maestro-Martínez, M., and Montserrat-Martí, G.: Leaf
482 morphology and leaf chemical composition in three Quercus (Fagaceae) species along a rainfall gradient in NE
483 Spain, Trees, 11, 127–134, https://doi.org/10.1007/PL00009662, 1997.

484 Chen, J. M. and Black, T. A.: Defining leaf area index for non-flat leaves, Plant Cell Environ., 15, 421–429,
485 https://doi.org/10.1111/j.1365-3040.1992.tb00992.x, 1992.

https://doi.org/10.5194/egusphere-2022-1055
Preprint. Discussion started: 14 October 2022

Disney, M.: Terrestrial LiDAR: a three-dimensional revolution in how we look at trees, New Phytol., 222, 1736–1741, https://doi.org/10.1111/nph.15517, 2018.

Gazal, R. M., Scott, R. L., Goodrich, D. C., and Williams, D. G.: Controls on transpiration in a semiarid riparian cottonwood forest, Agr. Forest Meterol., 137, 56–67, https://doi.org/10.1016/j.agrformet.2006.03.002, 2006.

Gower, S. T., Vogel, J. G., Norman, J. M., Kucharik, C. J., Steele, S. J., and Stow, T. K.: Carbon distribution and aboveground net primary production in aspen, jack pine, and black spruce stands in Saskatchewan and Manitoba, Canada, J. Geophys. Res., 102, 29029–29041, https://doi.org/10.1029/97JD02317, 1997.

Gower, S. T., Kucharik, C. J., and Norman, J. M.: Direct and Indirect Estimation of Leaf Area Index, fAPAR, and Net Primary Production of Terrestrial Ecosystems, Remote Sens. Environ., 70, 29–51, https://doi.org/10.1016/S0034-4257(99)00056-5, 1999.

Grotti, M., Calders, K., Origo, N., Puletti, N., Alivernini, A., Ferrara, C., and Chianucci, F.: An intensity, image-based method to estimate gap fraction, canopy openness and effective leaf area index from phase-shift terrestrial laser scanning, Agr. Forest Meterol., 280, 107766, https://doi.org/10.1016/j.agrformet.2019.107766, 2020.

Hardwick, S. R., Toumi, R., Pfeifer, M., Turner, E. C., Nilus, R., and Ewers, R. M.: The relationship between leaf area index and microclimate in tropical forest and oil palm plantation: Forest disturbance drives changes in microclimate, Agr. Forest Meterol., 201, 187–195, https://doi.org/10.1016/j.agrformet.2014.11.010, 2015.

Hijmans, R. J.: raster: Geographic Data Analysis and Modeling R package version 3.5-21, https://CRAN.R-project.org/package=raster., 2022.

Hosoi, F. and Omasa, K.: Voxel-Based 3-D Modeling of Individual Trees for Estimating Leaf Area Density Using High-Resolution Portable Scanning Lidar, IEE T. Geosci. Remote, 44, 3610–3618, https://doi.org/10.1109/TGRS.2006.881743, 2006.

Itakura, K. and Hosoi, F.: Voxel-based leaf area estimation from three-dimensional plant images, J. Agric. Meteorol., 75, 211–216, https://doi.org/10.2480/agrmet.d-19-00013, 2019.

Jonckheere, I., Fleck, S., Nackaerts, K., Muys, B., Coppin, P., Weiss, M., and Baret, F.: Review of methods for in situ leaf area index determination, Agr. Forest Meterol., 121, 19–35, https://doi.org/10.1016/j.agrformet.2003.08.027, 2004.

Jonckheere, I. G. C., Muys, B., and Coppin, P.: Allometry and evaluation of in situ optical LAI determination in Scots pine: a case study in Belgium, Tree Physiol., 25, 723–732, https://doi.org/10.1093/treephys/25.6.723, 2005.

Jucker, T., Bouriaud, O., Avacaritei, D., Dănilă, I., Duduman, G., Valladares, F., and Coomes, D. A.: Competition for light and water play contrasting roles in driving diversity-productivity relationships in Iberian forests, J. Ecol., 102, 1202–1213, https://doi.org/10.1111/1365-2745.12276, 2014.

https://doi.org/10.5194/egusphere-2022-1055
Preprint. Discussion started: 14 October 2022

518 Jump, A. S., Ruiz-Benito, P., Greenwood, S., Allen, C. D., Kitzberger, T., Fensham, R., Martínez-Vilalta, J.,
519 and Lloret, F.: Structural overshoot of tree growth with climate variability and the global spectrum of drought-
520 induced forest dieback, Glob. Change Biol., 23, 3742–3757, https://doi.org/10.1111/gcb.13636, 2017.

521 Jupp, D. L. B., Culvenor, D. S., Lovell, J. L., Newnham, G. J., Strahler, A. H., and Woodcock, C. E.: Estimating
522 forest LAI profiles and structural parameters using a ground-based laser called 'Echidna(R), Tree Physiol., 29,
523 171–181, https://doi.org/10.1093/treephys/tpn022, 2008.

524 Kamoske, A. G., Dahlin, K. M., Stark, S. C., and Serbin, S. P.: Leaf area density from airborne LiDAR:
525 Comparing sensors and resolutions in a temperate broadleaf forest ecosystem, Forest Ecol. Manag., 433, 364–
526 375, https://doi.org/10.1016/j.foreco.2018.11.017, 2019.

527 Kuusk, V., Niinemets, Ü., and Valladares, F.: A major trade-off between structural and photosynthetic
528 investments operative across plant and needle ages in three Mediterranean pines, Tree Physiol., 38, 543–557,
529 https://doi.org/10.1093/treephys/tpx139, 2018.

530 Leblanc, S. G. and Chen, J. M.: A practical scheme for correcting multiple scattering effects on optical LAI
531 measurements, Agr. Forest Meterol., 110, 125–139, https://doi.org/10.1016/S0168-1923(01)00284-2, 2001.

532 Lecigne, B., Delagrange, S., and Messier, C.: Exploring trees in three dimensions: VoxR, a novel voxel-based R
533 package dedicated to analysing the complex arrangement of tree crowns, Ann. Bot-London, 121, 589–601,
534 https://doi.org/10.1093/aob/mcx095, 2018.

535 Li, S., Dai, L., Wang, H., Wang, Y., He, Z., and Lin, S.: Estimating Leaf Area Density of Individual Trees
536 Using the Point Cloud Segmentation of Terrestrial LiDAR Data and a Voxel-Based Model, Remote Sens-Basel,
537 9, 1202, https://doi.org/10.3390/rs9111202, 2017.

538 Li, Y., Guo, Q., Tao, S., Zheng, G., Zhao, K., Xue, B., and Su, Y.: Derivation, Validation, and Sensitivity
539 Analysis of Terrestrial Laser Scanning-Based Leaf Area Index, Can. J. Remote Sens., 42, 719–729,
540 https://doi.org/10.1080/07038992.2016.1220829, 2016.

541 Lines, E. R., Fischer, F. J., Owen, H. J. F., and Jucker, T.: The shape of trees: Reimagining forest ecology in
542 three dimensions with remote sensing, J. Ecol., 110, 1730–1745, https://doi.org/10.1111/1365-2745.13944,
543 2022.

544 Long, J. N. and Smith, F. W.: Leaf area - sapwood area relations of lodgepole pine as influenced by stand
545 density and site index., Can. J. Forest Res., 18, 247–250, 1988.

546 López, R., Cano, F. J., Martin-StPaul, N. K., Cochard, H., and Choat, B.: Coordination of stem and leaf traits
547 define different strategies to regulate water loss and tolerance ranges to aridity, New Phytol., 230, 497–509,
548 https://doi.org/10.1111/nph.17185, 2021.

549 Lovell, J. L., Jupp, D. L. B., van Gorsel, E., Jimenez-Berni, J., Hopkinson, C., and Chasmer, L.: Foliage Profiles
550 from Ground Based Waveform and Discrete Point Lidar, SilviLaser, 1–9, 2011.

https://doi.org/10.5194/egusphere-2022-1055
Preprint. Discussion started: 14 October 2022

551 Ma, L., Zheng, G., Eitel, J. U. H., Magney, T. S., and Moskal, L. M.: Determining woody-to-total area ratio
552 using terrestrial laser scanning (TLS), Agr. Forest Meterol., 228–229, 217–228,
553 https://doi.org/10.1016/j.agrformet.2016.06.021, 2016.

554 Madrigal-González, J., Herrero, A., Ruiz-Benito, P., and Zavala, M. A.: Resilience to drought in a dry forest:
555 Insights from demographic rates, Forest Ecol. Manag., 389, 167–175,
556 https://doi.org/10.1016/j.foreco.2016.12.012, 2017.

557 Magnani, F., Mencuccini, M., and Grace, J.: Age-related decline in stand productivity: the role of structural
558 acclimation under hydraulic constraints, Plant Cell Environ., 23, 251–263, https://doi.org/10.1046/j.1365-
559 3040.2000.00537.x, 2000.

560 Mencuccini, M.: The ecological significance of long-distance water transport: short-term regulation, long-term
561 acclimation and the hydraulic costs of stature across plant life forms, Plant Cell Environ., 26, 163–182,
562 https://doi.org/10.1046/j.1365-3040.2003.00991.x, 2003.

563 Mencuccini, M. and Grace, J.: Climate influences the leaf area/sapwood area ratio in Scots pine, Tree Physiol.,
564 15, 1–10, https://doi.org/10.1093/treephys/15.1.1, 1995.

565 Monsi, M. and Saeki, T.: On the Factor Light in Plant Communities and its Importance for Matter Production,
566 Ann. Bot-London, 95, 549–567, https://doi.org/10.1093/aob/mci052, 1953.

567 Nakagawa, S., Johnson, P. C. D., and Schielzeth, H.: The coefficient of determination R2 and intra-class
568 correlation coefficient from generalized linear mixed-effects models revisited and expanded, J. R. Soc.
569 Interface, 14, 20170213, https://doi.org/10.1098/rsif.2017.0213, 2017.

570 Niinemets, Ü. and Valladares, F.: Tolerance to shade, drought, and waterlogging of temperate northern
571 hemisphere trees and shrubs, Ecol. Monogr., 76, 521–547, https://doi.org/10.1890/0012-
572 9615(2006)076[0521:TTSDAW]2.0.CO;2, 2006.

573 Niu, X., Fan, J., Luo, R., Fu, W., Yuan, H., and Du, M.: Continuous estimation of leaf area index and the
574 woody-to-total area ratio of two deciduous shrub canopies using fisheye webcams in a semiarid loessial region
575 of China, Ecol. Indic., 125, 107549, https://doi.org/10.1016/j.ecolind.2021.107549, 2021.

576 Olivas, P. C., Oberbauer, S. F., Clark, D. B., Clark, D. A., Ryan, M. G., O'Brien, J. J., and Ordoñez, H.:
577 Comparison of direct and indirect methods for assessing leaf area index across a tropical rain forest landscape,
578 Agr. Forest Meterol., 177, 110–116, https://doi.org/10.1016/j.agrformet.2013.04.010, 2013.

579 Owen, H. J. F., Flynn, W. R. M., and Lines, E. R.: Competitive drivers of inter-specific deviations of crown
580 morphology from theoretical predictions measured with Terrestrial Laser Scanning, J. Ecol., 109, 2612–2628,
581 https://doi.org/10.1111/1365-2745.13670, 2021.

582 Owen, H. J. F., Flynn, W. R. M., and Lines, E. R.: Individual TLS tree clouds collected from both Alto Tajo and
583 Cuellar in Spain., 2022.

https://doi.org/10.5194/egusphere-2022-1055
Preprint. Discussion started: 14 October 2022

584 Peppe, D. J., Royer, D. L., Cariglino, B., Oliver, S. Y., Newman, S., Leight, E., Enikolopov, G., Fernandez-
585 Burgos, M., Herrera, F., Adams, J. M., Correa, E., Currano, E. D., Erickson, J. M., Hinojosa, L. F., Hoganson, J.
586 W., Iglesias, A., Jaramillo, C. A., Johnson, K. R., Jordan, G. J., Kraft, N. J. B., Lovelock, E. C., Lusk, C. H.,
587 Niinemets, Ü., Peñuelas, J., Rapson, G., Wing, S. L., and Wright, I. J.: Sensitivity of leaf size and shape to
588 climate: global patterns and paleoclimatic applications, New Phytol., 190, 724–739,
589 https://doi.org/10.1111/j.1469-8137.2010.03615.x, 2011.

590 Pfeifer, M., Gonsamo, A., Disney, M., Pellikka, P., and Marchant, R.: Leaf area index for biomes of the Eastern
591 Arc Mountains: Landsat and SPOT observations along precipitation and altitude gradients, Remote Sens.
592 Environ., 118, 103–115, https://doi.org/10.1016/j.rse.2011.11.009, 2012.

593 Phillips, N., Bond, B. J., McDowell, N. G., Ryan, M. G., and Schauer, A.: Leaf area compounds height-related
594 hydraulic costs of water transport in Oregon White Oak trees, Funct. Ecol., 17, 832–840,
595 https://doi.org/10.1111/j.1365-2435.2003.00791.x, 2003.

596 Purves, D. and Pacala, S.: Predictive Models of Forest Dynamics, Science, 320, 1452–1453,
597 https://doi.org/10.1126/science.1155359, 2008.

598 Ridler, T. W. and Calvard, S.: Picture Thresholding Using an Iterative Selection Method, IEEE T. Syst. Man.
599 Cyb., 8, 630–632, https://doi.org/10.1109/TSMC.1978.4310039, 1978.

600 Sea, W. B., Choler, P., Beringer, J., Weinmann, R. A., Hutley, L. B., and Leuning, R.: Documenting
601 improvement in leaf area index estimates from MODIS using hemispherical photos for Australian savannas,
602 Agr. Forest Meterol., 151, 1453–1461, https://doi.org/10.1016/j.agrformet.2010.12.006, 2011.

603 Specht, R. L. and Specht, A.: Canopy structure in Eucalyptus-dominated communities in Australia along
604 climatic gradients, Canopy structure in Eucalyptus-dominated communities in Australia along climatic
605 gradients, 10, 191–213, 1989.

606 Vicari, M. B., Disney, M., Wilkes, P., Burt, A., Calders, K., and Woodgate, W.: Leaf and wood classification
607 framework for terrestrial LiDAR point clouds, Methods Ecol. Evol., 10, 680–694, https://doi.org/10.1111/2041-
608 210X.13144, 2019.

609 Warton, D. I., Wright, I. J., Falster, D. S., and Westoby, M.: Bivariate line-fitting methods for allometry, Biol.
610 Rev., 81, 259–291, https://doi.org/10.1017/S1464793106007007, 2006.

611 Warton, D. I., Duursma, R. A., Falster, D. S., and Taskinen, S.: smatr 3 - an R package for estimation and
612 inference about allometric lines: *The smatr 3 - an R package* , Methods Ecol. Evol., 3, 257–259,
613 https://doi.org/10.1111/j.2041-210X.2011.00153.x, 2012.

614 Weiss, M., Baret, F., Smith, G. J., Jonckheere, I., and Coppin, P.: Review of methods for in situ leaf area index
615 (LAI) determination, Agr. Forest Meterol., 121, 37–53, https://doi.org/10.1016/j.agrformet.2003.08.001, 2004.

https://doi.org/10.5194/egusphere-2022-1055
Preprint. Discussion started: 14 October 2022

616 Whitehead, D.: The Estimation of Foliage Area from Sapwood Basal Area in Scots Pine, Forestry, 51, 137–149,
617 https://doi.org/10.1093/forestry/51.2.137, 1978.

618 Wilkes, P., Lau, A., Disney, M., Calders, K., Burt, A., Gonzalez de Tanago, J., Bartholomeus, H., Brede, B., and
619 Herold, M.: Data acquisition considerations for Terrestrial Laser Scanning of forest plots, Remote Sensing of
620 Environment, 196, 140–153, https://doi.org/10.1016/j.rse.2017.04.030, 2017.

621 Woodgate, W., Jones, S. D., Suarez, L., Hill, M. J., Armston, J. D., Wilkes, P., Soto-Berelov, M., Haywood, A.,
622 and Mellor, A.: Understanding the variability in ground-based methods for retrieving canopy openness, gap
623 fraction, and leaf area index in diverse forest systems, Agr. Forest Meterol., 205, 83–95,
624 https://doi.org/10.1016/j.agrformet.2015.02.012, 2015.

625 Woodgate, W., Armston, J. D., Disney, M., Jones, S. D., Suarez, L., Hill, M. J., Wilkes, P., and Soto-Berelov,
626 M.: Quantifying the impact of woody material on leaf area index estimation from hemispherical photography
627 using 3D canopy simulations, Agr. Forest Meterol., 226–227, 1–12,
628 https://doi.org/10.1016/j.agrformet.2016.05.009, 2016.

629 Zhang, Y., Chen, J. M., and Miller, J. R.: Determining digital hemispherical photograph exposure for leaf area
630 index estimation, Agr. Forest Meterol., 133, 166–181, https://doi.org/10.1016/j.agrformet.2005.09.009, 2005.

631 Zheng, G., Moskal, L. M., and Kim, S.-H.: Retrieval of Effective Leaf Area Index in Heterogeneous Forests
632 With Terrestrial Laser Scanning, IEEE T. Geosci. Remote, 51, 777–786,
633 https://doi.org/10.1109/TGRS.2012.2205003, 2013.

634 Zhu, X., Skidmore, A. K., Wang, T., Liu, J., Darvishzadeh, R., Shi, Y., Premier, J., and Heurich, M.: Improving
635 leaf area index (LAI) estimation by correcting for clumping and woody effects using terrestrial laser scanning,
636 Agr. Forest Meterol., 263, 276–286, https://doi.org/10.1016/j.agrformet.2018.08.026, 2018.

637